Journal of Geochemical Exploration 196 (2019) 20–32

Contents lists available at ScienceDirect

Journal of Geochemical Exploration

journal homepage: www.elsevier.com/locate/gexplo

Mass balance and origin of fluids associated to smectite and chlorite/smectite alteration in Seival Mine Cu–Mineralization – Camaquã Basin – Brazil (Part II)

Eduardo Fontana[a,b,c,*], Christophe Renac[c], André S. Mexias[b], Aurélie Barats[c], Marie C. Gerbe[d], Rodrigo W. Lopes[b,c], Lauro V.S. Nardi[b]

[a] UFVJM – Universidade Federal dos Vales do Jequitinhonha e Mucuri, Centro de Geociências, Instituto de Ciência e Tecnologia, Rodovia MGT 367, Km 583, n° 5000 – Alto da Jacuba, Diamantina, MG, Brazil
[b] UFRGS – Universidade Federal do Rio Grande do Sul, Av. Bento Gonçalves 9500 – Agronomia, Porto Alegre, RS, Brazil
[c] Université Côte d'Azur, CNRS, OCA, IRD, Géoazur, 250 rue Albert Einstein, Sophia Antipolis, 06560 Valbonne, France
[d] Univ. Lyon, UJM–Saint–Etienne, CNRS, Laboratoire Magmas et Volcans UMR 6524, F–42023 Saint–Etienne, France

ARTICLE INFO

Keywords:
Copper deposits in volcano–sedimentary sequences
Chlorite–smectite
Mass balance
Meteoric–hydrothermal alteration
High–temperature copper deposits

ABSTRACT

The Seival Mine, located in the Camaquã Basin, hosts several small Cu and Ag ore deposits in volcano–sedimentary sequence surrounding the Lavras do Sul Intrusive Complex. Alteration minerals consist of calcite, sulfate, smectite and chlorite/smectite associated with Cu–rich sulfides. The mass balance calculations from less altered to altered volcanic rocks show large chemical changes with the mobility of mettallic elements in major or trace amounts. Mass balance calculations for similar volcanic protoliths, with different degrees of alteration or textural variations, indicate that increasing proportions of clay minerals reflects higher degrees of alteration. This alteration did not mobilize Si, Al, Fe, and Mg and had a small effect on other metallic elements such as Cu, Zn, Ni, and Au. Consequently, fluids associated with propylitic to argillic alteration with chlorite–smectite precipitation did not participate in the transport of base metals and ore deposition. Interpretations of oxygen stable–isotopes for magmatic, late magmatic and hydrothermal minerals show decreasing proportion magmatic fluid ($\delta^{18}O_{fluid}$ of andesine labradorite ca. 5 to 7‰), toward a predominance of meteoric fluid ($\delta^{18}O_{fluid}$ of quartz and calcite) between −12 and 0‰ for the low–temperature alteration (250 to 80 °C). Carbon stable isotopes result suggest a mixture of inorganic carbon ca. −7 to −5‰ from volcanic CO_2 with late carbonate precipitation with atmospheric signatures ca. −4 to −1‰. These mass balance and stable isotopes interpretations suggest that high–temperature late–magmatic fluid/rock interaction (650 to 350 °C) has promoted the base metal enrichment.

1. Introduction

The Camaquã Basin (Chemale Jr., 2000; Paim et al., 2000; Wildner et al., 2002), in the Rio Grande do Sul state hosts disseminated Cu, Zn, Pb, and Au deposits (Nardi and Lima, 1988; Veigel and Dardena, 1990; Mexias et al., 1990; Remus et al., 1997; Lima and Nardi, 1998; Remus et al., 2000; Mexias et al., 2007; Renac et al., 2014; Fontana et al., 2017). The Hilário Formation (Lima and Nardi, 1992; Lima, 1995; Paim et al., 2000) represents the largest area of exposed rocks in the Camaquã Basin, and in the study area it is located in the eastern part of Lavras do Sul plutonic rocks (Fig. 1). These volcanic rocks host the Seival Mine, exploited during the first half of XXth century (e.g., Lopes et al., 2014; Fontana et al., 2017). They consisted of small and disseminated Cu–sulfide and native Ag deposits (Total ca. 200 tons with Cu range from 0.5 to 2.5% and Ag ca. 15 to 70 $mg{\cdot}kg^{-1}$). The ore bodies are described as hydrothermal fluid circulation and ore deposition (Reischl, 1978). The source of metal is unidentified and could be related to the lava flows, andesitic dikes or monzonite intrusion from the near Lavras do Sul Intrusive Complex (Gastal and Lafon, 2006; Raposo and Gastal, 2009; Gastal et al., 2015).

Previous studies (Lopes et al., 2014; Fontana et al., 2017) identified magmatic to hydrothermal mineral assemblages. The different hydrothermal minerals form halos with smectite, chlorite/smectite mixed layer in lava flows, chlorite/smectite mixed layer, corrensite in the subvolcanic

* Corresponding author at: UFVJM – Universidade Federal dos Vales do Jequitinhonha e Mucuri, Centro de Geociências, Instituto de Ciência e Tecnologia, Rodovia MGT 367 – Km 583, n° 5000 – Alto da Jacuba, Diamantina, MG, Brazil.
E-mail addresses: eduardo.fontana@ict.ufvjm.edu.br (E. Fontana), christophe.renac@unice.fr (C. Renac), andre.mexias@ufrgs.br (A.S. Mexias), aurelie.barats@unice.fr (A. Barats), gerbe@univ-st-etienne.fr (M.C. Gerbe), rodrigo.winck@ufrgs.br (R.W. Lopes), lauro.nardi@ufrgs.br (L.V.S. Nardi).

https://doi.org/10.1016/j.gexplo.2018.10.001
Received 12 November 2017; Received in revised form 19 July 2018; Accepted 3 October 2018
Available online 06 October 2018

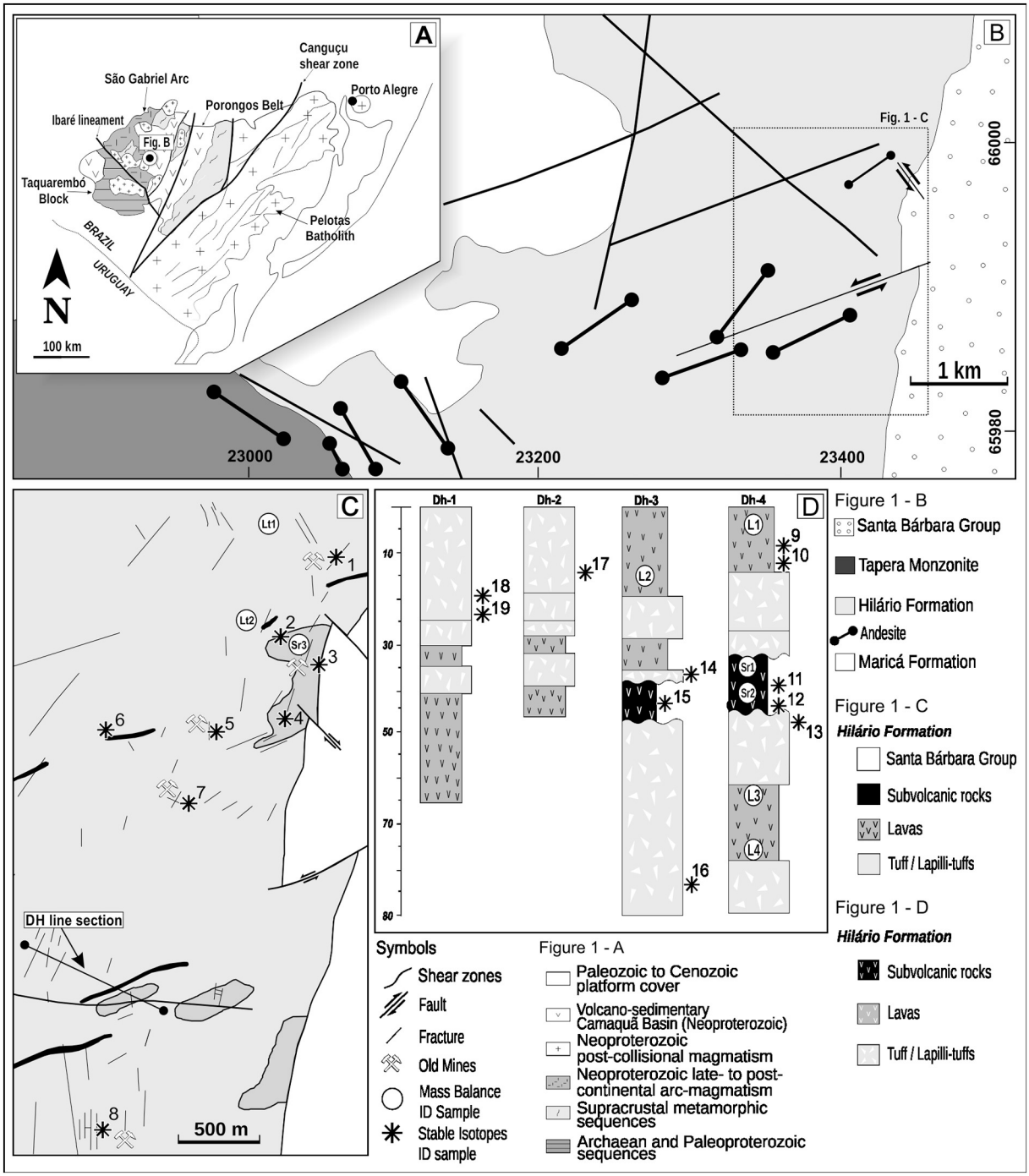

Fig. 1. A) Geotectonic units of southernmost Brazilian shield; B) Simplified geological map of Lavras do Sul plutonic and volcanic rocks of Hilário Formation; C) Sample location after Fontana et al., 2017). The volcanoclastic rocks of Seival Mine: Lt1 and 2 = lapilli tuff; L1, 2, 3 and 4 = lava flows; Sr1, 2 and 3 = subvolcanic rocks and DH = drill hole.

rocks, and chlorite in fractured zones associated with Cu–rich sulfide, barite, calcite and hematite (Lopes et al., 2014; Fontana et al., 2017). In the context of base–metal deposits, the formation of clay minerals frequently associated with the transport of fluids with chemical elements. These fluxes of matter vary with temperature (Capuano, 1992; Jiang et al., 1994), origin of fluids and changes of water/rock ratios (Henley, 1985; Sillitoe, 2010; Chiodini et al., 2011; Cruz et al., 2015). The temperatures change from high to low–temperatures with albitization (650 to 350 °C, Hövelmann et al., 2010; Kaur et al., 2012) to chlorite and smectite (250 to 80 °C, Tardy et al., 1987; De Caritat et al., 1993; Schleicher et al., 2012). The fluids can be related to lava cooling (late–magmatic), dikes emplacement with magmatic fluids or influx of meteoric–hydrothermal water. This paper attempts to combine clay mineralogy and geochemical changes of whole–rocks to estimate real gain and loss of chemical elements during the hydrothermal alteration and Cu-Ag metal deposition. Further, stable isotope values of magmatic and hydrothermal minerals estimate the magmatic or meteoric origin of fluids.

2. Geological settings and hydrothermal alteration

The studied area is part of the southern Brazilian shield which is compartmented in four geotectonic units: Taquarembó Block; São

Gabriel Arch; Porongos Belt; Pelotas Batholith and subordinate metamorphic rocks (Fig. 1A and the references cited in Fontana et al., 2017). The emplacement and filling with volcanoclastic sediments of the Camaquã Basin is related to the transcurrent tectonic regime and the magmatic activity during the Ediacaran times (Hallinan et al., 1993; Chemale Jr. et al., 1995; Chemale Jr., 2000; Saalmann et al., 2005; Philipp et al., 2007; Saalmann et al., 2007; Hartmann et al., 2011; Saalmann et al., 2011). The Seival area is part of Hilário Formation (Nardi and Lima, 1985) located on the western side of the Camaquã Basin in contact with the Lavras do Sul intrusive complex (Fig. 1B, C, and D). The Seival lithology consists of lapilli tuff, lava flows and subvolcanic rocks with trachytic to andesitic mineralogy (Lopes et al., 2014; Fontana et al., 2017). Albite or smectite (S), chlorite/smectite (C/S), and corrensite (Co) and calcite vary in proportion. They replace magmatic feldspars, pyroxenes, and intergranular glass from lava flows, lapilli tuff (S and C/S), and subvolcanic rocks with corrensite (cf., Fontana et al., 2017).

3. Methods

3.1. Sampling and preliminary consideration

Preliminary petrography of these materials revealed heterogeneous volcanoclastic textures with variable proportions of magmatic phenocrysts and microlites or alteration minerals (smectite, chlorite/smectite, several generations of calcite) (Lopes et al., 2014; Fontana et al., 2017). We examined texture and mineralogy of each sample in thin sections completed with Scanning Electron Microscopy (SEM) with Energy Dispersive Spectroscopy (EDS), and X–Ray Diffraction (XRD) of clay–size separates. Samples selected came from lava flows, lapilli tuff, and subvolcanic rocks described in the first part of this work (Fontana et al., 2017).

The lava flows have a trachytic texture with matrix that contains relictual plagioclase (Pl), pyroxene (Px), glass and microliths of feldspars replaced by quartz, clay minerals, carbonate with minor epidote + titanite, iron oxides, euhedral pyrite, and vesicles filled by green clay minerals, and quartz or carbonate. The lapilli tuff, is composed by Pl, Px, and clasts of andesitic rocks with a matrix containing a mixture of clay minerals and carbonate, oxides, chalcocite + bornite, and barite. The subvolcanic rocks containing phenocrysts of Pl and smaller Px, the clay minerals fill vesicles and the matrix is composed by microliths of Pl, particularly the phenocrysts, are transformed to albite–epidote + titanite–"sericite"– and carbonates (Fig. 2A, in Table 1 and Fig. 1; Fontana et al., 2017). Among the eleven field samples and thirteen cores observed, we selected four lava flows (L1 – L2 and L3 – L4), two lapilli tuff (Lt1 – Lt2) and three subvolcanic rocks (Sr1 – Sr2 and Sr3; Table 1). The different textures present different degrees of alteration but came from vicinal locations (Fig. 1C and D).

3.2. Density, loss on ignition, major, and trace element in whole–rocks

Samples were broken to collect the fragments with similar textures, avoiding veins and vesicles. Density measured on cubic centimeter sample covered with hot paraffin (error ± 0.02, 4 measurements). One gram of the sample was heated at 1050 °C for 4 h to measure the Loss On Ignition (LOI). This LOI was combined with elemental analyses of volatile (Dumas combustion) to quantify sulfur and carbon (C_{tot}) contents or CO_2 equivalent ($C_{tot} \times 0.273$). Carbonate proportions were measured by the volume of CO_2 released by acid digestion (hydrochloric acid = 2 mol L^{-1} with on 0.5 g of powdered sample). The comparison of $CO_{2\ (volume)}$ and C_{tot} allowing the identification of carbonate and graphite.

The powdered rocks were first fused and analyzed for major and trace elements in the Activation Laboratories Ltd., Ontario, Canada. Quantification and quality control was realized with external standards BHVO–1 and BCR (provided by ACME–lab). Major element concentration are expressed in % with relative errors between 1 and 2% or SiO_2, Al_2O_3, Fe_2O_3, K_2O and CaO (quantification limits of 0.05%) and 5% for Na_2O, MgO, TiO_2, and P_2O_5. The Trace Elements (TE) and Rare Earth Elements (REE) were measured on the fused bead by laser ablation (BHVO–1 external standard). Powdered samples and external standard (BHVO–1) were also acid digested with HF (20 N, Ultrapure) and HNO_3 (5 N, Ultrapure), diluted in 1% HNO_3 solution and analyzed by Inductively Coupled Plasma Mass Spectrometry (ICPMS, ELAN DRCII, Perkin Elmer). External and internal calibrations were performed using multielemental solutions and internal standards: Ge, In and Re chosen according to the targeted mass. Concentration is expressed in mg/kg (ppm) with a limit of quantification of fifty picogram $kg^{-}1$ (ng/kg). Significant chemical change are related to the individual uncertainty of each element related to dilution (0.1 mg), density: (± 0.02), major contents with 2% (2σ error), minor, and trace elements 5% (2σ error) below 0.1 mg/kg. These individual errors and error propagation have been further used to compare initial concentration (C_i^0 = parent rock) to altered rock (C_i) in mass balance calculations. The calculation of error propagation indicates meaningful changes for individual variations higher than ca. 0.2 wt%: wt% for major elements, 2 mg/kg for trace elements, and relative changes higher than ± 0.15% ($\Delta C_i/C_i^0$ = C(daughter − parent) / Ci^0 (parent); cf.,Gresens, 1967; Grant, 1986).

3.3. Mineral separation and stable isotope measurements

The mineral separates consist of an aliquot of silicates extracted from phenocrysts and concentrates of microlithic plagioclase, purified through magnetic fields, bromoform ($CHBr_3$) and mixtures of bromoform and ethanol for heavy liquid separation. The concentrates of pyroxene and plagioclase washed with acetone, ethanol and deionized water, then observed with a binocular microscope and grains handpicked. We collected calcite (Fontana et al., 2017) in veinlets and vesicles by micro–drilling. The euhedral quartz crystals (crystal size: 0.1 mm) in carbonate vein (mm), handpicked after acid digestion of carbonates (Cal–1 from vesicle; Cal–2 and –3 from veins; cf., Fontana et al., 2017). Mineral separations and purification did not allow collection of pure smectite, chlorite/smectite or corrensite. However, several tens of altered pyroxene grains allow the collection of chlorite/smectite (XRD). We observed and checked the mineralogy of all separated phases by SEM–EDS, and XRD techniques.

The stable isotopes values of oxygen ($\delta^{18}O$) and carbon ($\delta^{13}C$) were obtained of CO_2 extracted from calcite (McCrea, 1950) and O_2 liberated with BrF_5 from silicates and converted to CO_2 (Clayton and Mayeda, 1963). The CO_2 was analyzed with Gas–source mass spectrometer (Micromass Isoprime, Université Jean Monnet). Stable isotope values of calcite ($\delta^{13}C_{cal}$ and $\delta^{18}O_{cal}$), quartz, pyroxene, chlorite/smectite, and feldspars ($\delta^{18}O_{qtz}$ to $\delta^{18}O_{feldspar}$) are reported as per mil (‰) relative to V–PDB for carbon and V–SMOW for oxygen. The analytical error and reproducibility for the standards and replicates are $\delta^{18}O_{silicate}$ ± 0.3‰, $\delta^{18}O_{carbonate}$ ± 0.2‰ and $\delta^{13}C_{carbonate}$ ± 0.06‰ (2σ).

4. Results

4.1. Petrography mineralogy and crystallography

The alteration is preliminarily estimated from the gray, dark and light green colors of lava flows (L), lapilli tuff (Lt), and subvolcanic rocks (Sr). The studied samples are for lava flows (L1 ➔ L2 and L3 ➔ L4), lapilli tuff (Lt1 ➔ Lt2) and subvolcanic rocks (Sr1 ➔ Sr2), with an arrow representing the macroscopic changes from less toward more altered rocks. Their petrographic and SEM–EDS observations allow identification of andesine–labradorite and augite phenocrysts of lava flows (Fig. 2B and C) with a low–proportion of phenocrysts in lapilli tuff samples. In the lapilli tuff, chlorite/smectite and calcite (Fig. 2) replaced the pyroxene with scarce fragments of pyroxene preserved. The phenocrysts of plagioclase are partially replaced by albite, minor epidote, iron oxides, and clay minerals in the subvolcanic rocks. The

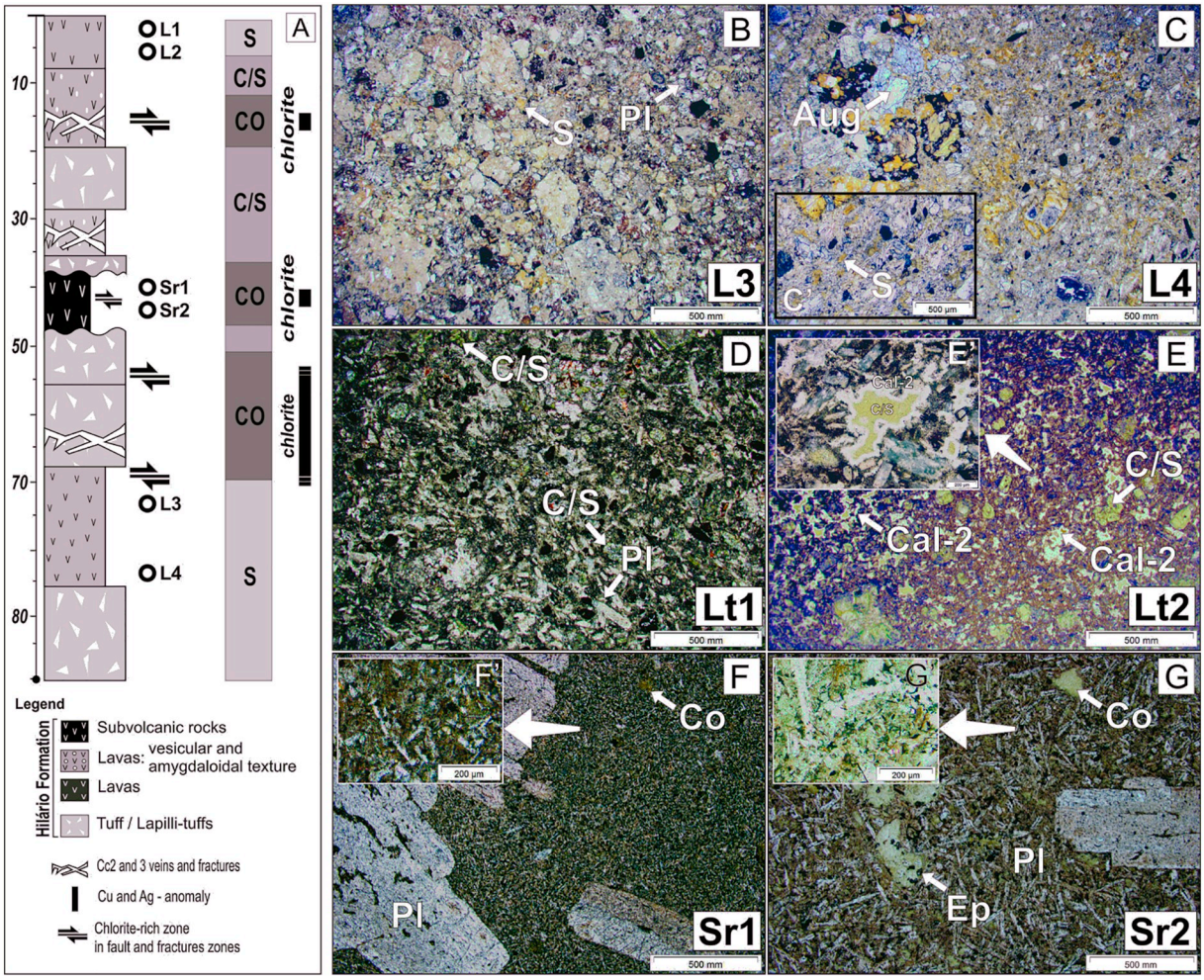

Fig. 2. A) Simplified stratigraphic column presents the major sedimentological changes in the Seival area. Adapted from: Lopes et al., 2014 and Fontana et al., 2017; B and C) photomicrographs of lava flows samples (L3 and L4) and detail (C') smectite material replacing glass and filling porosity; D and E) lapilli tuff samples (Lt1 and Lt2) and detail (E') Cal–2 and C/S material filling vesicles; F and G) subvolcanic rocks (samples: Sr1 and Sr2) and detail (F') matrix filled with plagioclase/corrensite minerals and G' matrix with corrensite–rich materials. Pl = plagioclase; Ep = epidote Cal = calcite; S = smectite (saponite); Chlorite/smectite = chlorite/smectite mixed–layer.

phenocrysts of pyroxene from lava flows have a dominant light green color.

The dark and light green matrixes consisted of albite microliths, clay minerals, calcite with minor iron oxide, and quartz. The macroscopic green staining of rocks is due to the different proportions of smectite and chlorite/smectite, replacing glassy matrix, and filling micrometer size vesicles (Fig. 2D, E, F, and G) associated with small proportions of quartz, and calcite. The crystallography of clay minerals varies with textures of volcanic rocks: smectite (L3, L4) and smectite–rich chlorite/smectite (L1, L2) in lava flows, chlorite/smectite in lapilli tuff (Lt1, Lt2), and corrensite in subvolcanic rocks (Sr1, Sr2). These precipitations of clay minerals contributed to mass and volume changes.

4.2. Whole–rock chemistry and apparent chemical changes associated with alteration

The albitized and smectite–rich lava flows (L3 ➔ L4) have a similar amount of LOI (6.6 wt%, wt%) and density (d = 2.58). This combination of alteration shows apparent gains of Na_2O and K_2O, Ni (35 mg/kg), Zr and losses of elements SiO_2, Fe_2O_3, CaO and MgO with Ba (80 mg/kg), Rb and Cu at tens of ppm and Au at ppm level. The chlorite/smectite and calcite–rich lava flows have similar LOI (L2 ➔ L1 with 6 to 8 wt%) and density (d = 2.65 and 2.63 ± 0.02). Whereas, lapilli tuff with chlorite/smectite and calcite have a higher LOI (Lt2 ➔ Lt1, 8 to 10 wt%; d = 2.62 and 2.59 ± 0.02). This increasing LOI (+1.9 wt%, Lt2 ➔ Lt1) is related to chlorite/smectite and a larger proportion of calcite as show CaO (+2.6 wt%), C_{tot} (+0.55 wt% equivalent to 2.3 wt% of CO_2) and 2.5 wt% of carbonate (e.g., acid digestion). The other apparent gains are Al_2O_3 and K_2O (ca. % level or + 0.1 wt%) and Sr, Ba, Rb (100 to 10 ppm) Ni, Co, Pb, U, La, and Ce elements. The apparent losses of chemical elements in altered lapilli tuff are SiO_2, Na_2O, and Fe_2O_3, MgO (> −0.7 wt%) associated with Cu and Pb and even smaller losses of Medium and Heavy Rare Earth Elements. The subvolcanic rocks with corrensite and calcite (Sr1 ➔ Sr2) have the lowest LOI of altered volcanic rocks (LOI: 3 to 3.9 wt%). The LOI increase is associated with apparent gains of MgO (0.7 wt%), Sr (50 mg/kg), and a smaller increase of Cu, Rb, and Ni (ppm). Like lava flows (L) and lapilli tuff (Lt), the subvolcanic rocks (Sr) with increasing degree of alteration show loss of SiO_2 (−3 wt%), Al_2O_3 and Fe_2O_3 (−0.7 wt%), Na_2O (−0.4 wt%), CaO (−2 wt%), Zn, Au (10 ppm), and REE contents.

4.3. C and O stables isotopes values of silicates carbonates

Purified fragments of pyroxene and feldspars from the matrix consist of augite and andesine–labradorite–rich and albite–rich plagioclase, respectively. The $\delta\ ^{18}O$ values of altered phenocrysts of pyroxene coming from lava flows (Location 2) vary from 8.5 to 11.1‰. The andesine–oligoclase–rich separates have $\delta^{18}O_{andesine–labradorite}$ values

Table 1
Major (%) and trace concentrations (ppm) from lava flows (L), lapilli tuff (Lt), and subvolcanic rocks (Sr) used for mass balance calculation.

	Lava	Subvolcanic rocks			Lavas				Lapilli-tuff	
wt%	NAR[a]	Sr1	Sr2	Sr3	L3	L4	L1	L2	Lt1	Lt2
SiO_2	55.7	56.2	55.6	57.1	55.6	54.7	49.1	49.4	52.4	49.7
Al_2O_3	18.3	18	18	18.5	12	12.5	13.6	14.6	13.8	14.3
K_2O	2.4	1.6	1.6	5.2	1.6	1.9	1.5	1.7	1.7	2.1
CaO	6.2	2.1	2	1.1	5.4	5.4	10	7.3	7.9	10.5
Na_2O	4.1	7.1	6.9	5.4	2.8	3.2	3.2	3.2	4	2.9
MgO	2.8	4.4	4.7	0.5	7.7	7.9	5.5	7.5	3.5	2.8
Fe_2O_{3T}	5.8	5.8	5.4	8.6	6.9	6.5	6	8.3	7.1	6.2
MnO	0.1	0.1	0.1	0	0.1	0.1	0.2	0.1	0.2	0.1
TiO_2	0.9	1	0.9	0.8	0.6	0.6	0.8	0.8	0.7	0.7
P_2O_5	0.3	0.5	0.4	0.3	0.3	0.3	0.3	0.3	0.3	0.3
LOI	2.2	3	3.9	1.9	6.6	6.6	9.7	6.4	8.1	10
$\%C_{Total}$	0.36	0.06	0.06	0.1	0.17	0.11	1.93	0.43	1.44	2.06
$\%S_{Total}$	0.3	< 0.02	< 0.02	< 0.02	0.1	< 0.02	< 0.02	< 0.02	< 0.02	< 0.02
ppm										
Ba	1671	394	411	3270	684	797	410	794	844	880
Sr	1200	428	499	896	722	753	508	753	535	775
Rb	49.8	35.6	39.4	131.5	28.8	32.3	26.7	34.7	30.6	46.3
Cs	N.A.	3.1	3	5	1.1	1	2.1	1.5	1.8	3.4
Ta	N.A.	112	104	0.3	0.4	0.4	0.5	0.5	108	109
Nb	22	10.8	10.8	7.5	7.3	7.4	7	7.4	7.9	8.7
Th	N.A.	12.3	11.5	6.5	5.2	5.5	4.8	5.6	5.9	7
U	N.A.	4.5	4.3	2.2	2.1	2.2	1.9	2.3	2	2.6
Zr	296	190	189	145	124	126	129	144	137	155
V	N.A.	13.9	13.4	162	99	100	128	134	26.2	30.2
Ga	N.A.	5.6	4.1	21.3	16.7	17.2	15.9	18.6	4.7	5.2
Sc	N.A.	N.A	N.A	13	15	14	17	17	N.A	N.A

		SR			L				LT	
ppm	NAR[b]	Sr1	Sr2	Sr3	L3	L4	L1	L2	Lt1	Lt2
Cu	N.A	231	141	2.1	28.4	33.9	48.4	30.9	62	35
Mo	N.A	0.9	0.4	0.3	0.5	0.6	< 0.1	0.5	0.3	0.4
Sn	N.A	2	2	1	1	1	1	1	1	2
W	N.A	0.9	0.7	1.4	1.1	< 0.5	0.8	0.6	0.5	1
Zn	N.A	21.8	23	22	61	60	137	76	18.1	18.8
Pb	N.A	3.7	2.8	14.1	11.7	10.4	4.7	28.7	7.7	14.3
Ag	N.A	0.5	0.5	< 0.1	< 0.1	< 0.1	< 0.1	< 0.1	< 0.1	< 0.1
Ni	22.5	317	363.5	42.1	201.2	175.2	108.2	92.5	27.1	22.9
Co	24.7	8.6	10.3	13	30.7	32	28.8	32	158.1	175.7
Se	N.A	< 0.5	< 0.5	< 0.5	1	< 0.5	< 0.5	< 0.5	< 0.5	< 0.5
As	N.A	5.6	4.1	14.5	19.8	4.2	1.2	5.4	4.7	5.2
Sb	N.A	0.2	< 0.1	0.6	< 0.1	0.1	< 0.1	0.4	< 0.1	0.1
Li	N.A	N.A	N.A	N.A	N.A	N.A	N.A	N.A	N.A	N.A
Tl	N.A	< 0.1	< 0.1	< 0.1	0.2	0.2	< 0.1	< 0.1	< 0.1	< 0.1
Hg	N.A	0.3	0.2	< 0.01	0.3	0.1	0	0	< 0.01	< 0.01
Au[c]	N.A	7.2	4.4	< 0.5	< 0.5	1.5	1.9	< 0.5	1.8	0.8
La	52.1	46.2	42.2	51.9	30.7	31.5	33.6	35.7	31.4	34.6
Ce	102.7	97.1	93.7	86.7	59.5	61.2	63.3	65.4	64.9	68.7
Pr	10.6	11.1	11.1	10.5	6.9	7.1	7.9	7.8	7.6	7.8
Nd	43.2	42	42.6	37.9	26.8	27.8	29.9	30.5	29.7	29.6
Sm	8.9	7.3	7.4	7.3	4.8	4.7	5.5	5.5	5.4	5.2
Eu	2	1.8	2	2	1.2	1.2	1.5	1.6	1.6	1.4
Gd	6.5	5	5.2	5.6	3.4	3.4	4.4	4.3	4	3.7
Tb	N.A	0.7	0.7	0.7	0.5	0.5	0.6	0.6	0.5	0.5
Dy	3.9	3.3	3.3	3.2	2.1	2.1	2.8	3.1	2.8	2.4
Ho	0.7	0.6	0.6	0.6	0.4	0.4	0.5	0.6	0.5	0.5
Er	1.9	1.5	1.5	1.6	1.1	1.2	1.5	1.6	1.4	1.2
Tm	0.3	0.2	0.2	0.2	0.2	0.2	0.2	0.2	0.2	0.2
Yb	1.5	1.5	1.4	1.3	1	1.1	1.3	1.4	1.2	1.1
Lu	0.2	0.2	0.2	0.2	0.2	0.2	0.2	0.2	0.2	0.2
La/Yb	34.7	31.9	29.9	41.2	31.6	28.4	25.8	25.7	26.2	32.6
Eu/Eu[b]	0.8	0.9	1	0.9	0.9	0.9	1	1	1	1
ΣREE	234.5	218.4	212	209.7	138.8	142.6	153.2	158.4	151.4	157.1

[a] Nonaltered andesitic rocks from Hilário Formation (Liz et al., 2008).
[b] Nonaltered andesitic rocks from Hilário Formation (Liz et al., 2008).
[c] Values for Au = ppb.

ranging from 6.6 to 8.1‰ and albite–rich plagioclase $\delta^{18}O_{albite-rich}$ between 14.2 and 16.2‰ (Table 4). The chlorite/smectite extracted from altered lava flows have $\delta\ ^{18}O_{values}$ between 23.8 and 27.8‰. Euhedral quartz in vesicle and veinlets have $\delta^{18}O_{qtz}$ varying from 19.2 to 24‰, except one value of 17.6‰. The sampling of calcite was realized using (Cal–1 to –3) described in petrographic observations (Fontana et al., 2017) in the vesicles (Cal–1) and veins (Cal–2 and Cal–3; cf., Fontana et al., 2017). The $\delta^{13}C_{cal}$ and $\delta^{18}O_{cal}$ values vary from −7.1 to −1.7‰ V–PDB ($\delta^{13}C_{cal}$) and from 7.5 to 19.8‰ V–SMOW ($\delta^{18}O_{cal}$) (Table 4). The $\delta^{13}C_{cal}$ and $\delta^{18}O_{cal}$ values coming from calcite in altered pyroxene have values similar to those in veins (Cal–2 and –3).

5. Discussion

5.1. Mineralogical changes associated with late–magmatism to hydrothermal stages

The X–ray diffraction (XRD) recognized similar to clay minerals as the study of eighty samples with smectite and smectite–rich chlorite/smectite in lava flows (L), chlorite/smectite in lapilli tuff (Lt), and corrensite (Sr) in andesitic dikes. Like proposed by Fontana et al. (2017), the homogeneous occurrence of smectite–rich clays in lava flows, chlorite/smectite in lapilli tuffs and corrensite in andesitic dikes suggest hydrothermal alteration controlled by lithotypes (L, Lt, and Sr). However, in situ observation with optical and electronic microscopy show size and small compositional changes from grain to grain. These local changes suggest continuous or different in–situ reactions. Nevertheless, the altered pyroxene (Location 2) are homogeneously composed of chlorite and chlorite/smectite (XRD) with a small proportion of calcite. This pyroxene alteration to chlorite and chlorite/smectite suggest local equilibrium compare to chlorite/smectite homogeneously filling the porosity of lava flows and sub–volcanic rocks.

All lithotypes studied are plotted in different empirical geochemical indexes that describe the intensity of hydrothermal alteration. The results for Pearce Element Ratio (PER, e.g., MacLean, 1990; Huston, 1993; Stanley and Madeisky, 1994; Barrett and MacLean, 1999), alteration index of 26 to 54% (Ishikawa et al., 1976), and chlorite–carbonate–pyrite *index* (Large et al., 2001) of 46 to 77% are presented in Fig. 3; Table 1 and Supplementary material (*Mass Balance ISOCON – Diagrams*). These different diagrams and indexes suggest a mild alteration of alkali feldspar or pyroxene but do not indicate a dominant reaction of pervasive alteration. The preliminary comparison of apparent less to more altered rocks (lava flows, lapilli tuff, and subvolcanic rocks) suggest the increasing proportion of LOI, CaO, and C_{tot} (L1 to L2) and MgO, Fe_2O_3 (L3 to L4), respectively related to calcite and chlorite–rich clays with iron oxides. Nevertheless, the SiO_2/Al_2O_3 wt% ratios of whole–rocks from 3 to 4.6 (Table 1 and supplementary material – *Mass Balance ISOCON – Diagrams*) higher than clay minerals (smectite: 3.5; chlorite/smectite: 2.8 to 3.1) due to the contribution high–Si phase such quartz and albite. Consequently, the hydrothermal alteration in the Seival is a sum of hydrothermal reactions with andesine to oligoclase + augite and glass to albite + clay minerals + quartz, and carbonates.

5.2. Mass balance calculation and isocompositional calculations (Isocon) with Al_2O_3 constant

The predominance of hydrothermal alteration with alumina–silicate (clay minerals and albite) and quartz with minor calcite or disseminated sulfides suggests mild acidic fluids (Vaughan and Corkhill, 2017). These acidic fluids would circulate from degassing magma to meteoric water influx. Therefore, we calculated chemical mass balance (EasyGresGrant; López-Moro, 2012) assuming Al and Ti as immobile elements which correspond to mild acidic to neutral pH of fluids. The assumption of constant concentrations of Al_2O_3 and TiO_2 from fresh to altered rocks (Tables 2 and 3; Supplementary material *Mass Balance ISOCON – Diagrams*) allowed

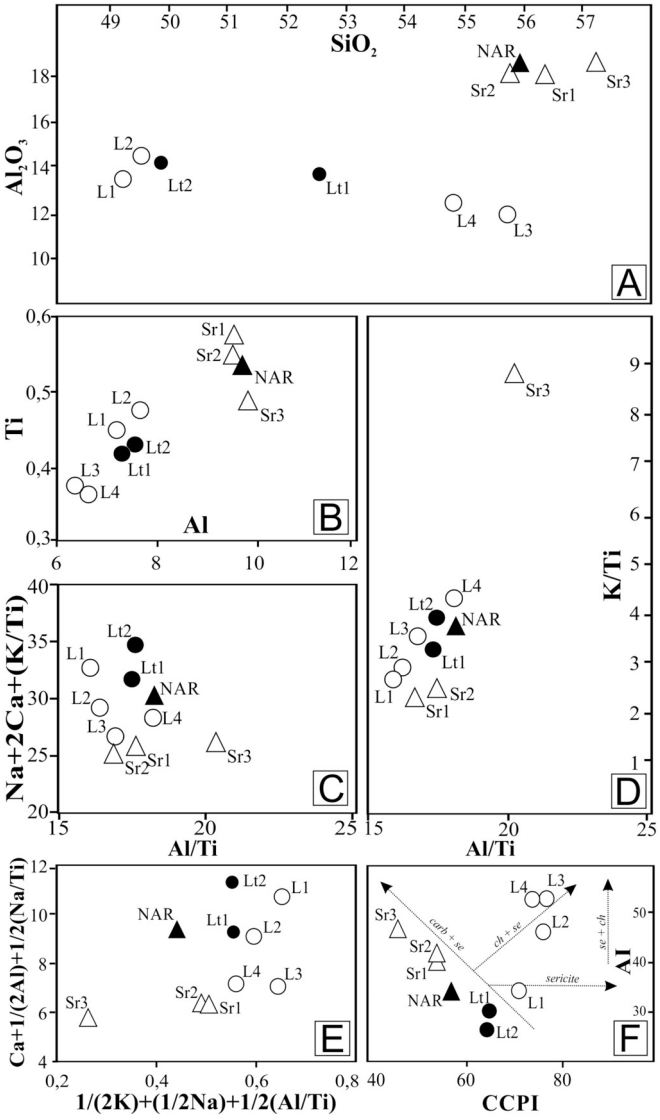

Fig. 3. Oxide and molar ratios for geochemical diagrams based on major and trace elements (PER/GER diagrams, A and B) and alteration box diagram AI vs. CCPI (Pearce, 1968, 1987; Ishikawa et al., 1976; Large et al., 2001). The name of samples used (Figs. 1 and 2) is (white triangle) = subvolcanic rocks; (dark triangle) = less altered volcanic rocks (Table 1 and Fontana et al., 2017); (white circle) = drill hole samples of effusive lava flows; (dark circle) = lapilli tuff samples; NAR (Liz et al., 2008).

calculation of concentration changes (i) and constant mass or volume (ii). In the case (i), we calculated gain and loss of mobile elements between a parent and daughter rocks ($\Delta Ci/Ci^0$ = (daughter − parent) / Ci^0 parent); Table 2). Furthermore, $\Delta Ci/Ci^0$ and Isocon slopes (Gresens, 1967; Grant, 1986; MacLean, 1990; Huston, 1993; Stanley and Madeisky, 1994; López-Moro, 2012) allowed calculation of enrichment or dilution factor related to mass or volume (ii).

The chemical compositions (Table 1) of whole–rock with LOI > 1.9 wt% indicate altered materials. Consequently, none of the samples from the Seival area can be used as a not altered protolith (Parent rock). A bibliographic survey of mineralogy and composition of trachybasalts and andesite in the Lavras do Sul and Camaquã Basin identified a small number of andesitic rocks with low LOI. The best candidate for a parent rock (Table 2) is the not–altered rocks (NAR) – the andesite average composition presented by Fontana et al. (2017) after Liz et al. (2008) data compilation. However, this mass balance calculations indicate unrealistic gains (+50%) of volume. These unrealistic changes suggest

Table 2
Summary of mass balance calculation from Sr3 LOI > 1.9 wt% to lava flows and subvolcanic rocks associated with smectite (L3), Chlorite/smectite + calcite (L1) and corrensite + calcite (Sr2). Indicated values represent changes of gains and losses above the analytical uncertainty or error propagation.

Sr3 → L3				Δ volume = 50%		Sr3 → L1				Δ volume = 30%		Sr3 → Sr2				Δ volume = −1%	
S altered lava				Δ mass = 52%		C/S + calcite altered lava				Δ mass = 35%		Co + calcite altered lava				Δ mass = +1%	
Constant volume	$\Delta C_i/C_i^0$	ΔC_i	Constant Al content	$\Delta C_i/C_i^0$	ΔC_i	Constant volume	$\Delta C_i/C_i^0$	ΔC_i	Constant Al content	$\Delta C_i/C_i^0$	ΔC_i	Constant volume	$\Delta C_i/C_i^0$	ΔC_i	Constant Al content	$\Delta C_i/C_i^0$	ΔC_i
Gain		%															
			SiO2	0.48	27.69				**CaO**	11.23	12.36						
			MgO	22.49	11.24				**LOI**	5.87	11.15						
						CaO	8.41	9.25	**SiO_2**	0.16	8.97						
MgO	14.64	7.32	**LOI**	4.3	8.17	**LOI**	4.29	8.14	**MgO**	13.8	6.9	**MgO**	8.68	4.34	**MgO**	8.56	4.28
LOI	2.53	4.8	**CaO**	6.49	7.14	**MgO**	10.39	5.19	**$\%C_{TOTAL}$**	24.97	2.5	**LOI**	1.11	2.11	**LOI**	1.08	2.06
CaO	3.99	4.39	**Fe_2O3**	0.81	4.72	**$\%C_{TOTAL}$**	18.98	1.9	**$\%C_{TOTAL}$**	***CO_2 equivalent***	*9.25*	**CaO**	0.91	1.00	**Na_2O**	0.3	1.62
Fe_2O3	0.21	1.21				**$\%C_{TOTAL}$**	***CO_2 equivalent***	*7.03*	**Fe_2O3**	0.39	2.27	**Na_2O**	0.32	1.71	**CaO**	0.88	0.97
		ppm															
Ni	3.85	162.27	**Ni**	6.29	264.73	**Zn**	5.45	119.85				**Cu**	176.87	371.42	**Cu**	174.59	366.64
			Sr	0.23	206.02				**Zn**	7.38	162.35	**Zn**	5.59	122.89	**Zn**	5.5	121.03
			Zn	3.23	71.03	**Ni**	1.66	69.93	**Ni**	2.46	103.49	**Zr**	0.34	49.43			
Zn	1.82	39.96	**Zr**	0.31	44.77	**Cu**	22.86	48.01	**Cu**	30.01	63.03				**Zr**	0.32	46.93
Cu	12.74	26.75	**Cu**	19.62	41.21				**Zr**	0.2	28.99						
Co	1.4	18.18	**Co**	2.6	33.82	**Co**	1.29	16.82	**Co**	1.98	25.75						
			Sc	0.76	9.88				**Sc**	0.76	9.88	**Ce**	0.11	9.58			
						Sc	0.35	4.6				**Nd**	0.15	5.87	**Nd**	0.14	5.31
			Ga	0.2	4.17							**Th**	0.82	5.32	**Th**	0.79	5.17
			Pb	0.27	3.74							**Au**	8.04	4.02	**Au**	7.93	3.96
			Nb	0.48	3.63				**Au**	4.11	2.06	**Nb**	0.48	3.6	**Nb**	0.46	3.46
LOSS		%															
Al_2O_3	−0.33	−6.11	**Al_2O_3**	**cst**		**Al_2O_3**	−0.23	−4.22	**Al_2O_3**	**cst**					**Al_2O_3**	**cst**	
K_2O	−0.69	−3.57	**K_2O**	−0.53	−2.76	**K_2O**	−0.7	−3.65	**K_2O**	−0.61	−3.18	**K_2O**	−0.68	−3.55	**K_2O**	−0.69	−3.57
Na_2O	−0.47	−2.56	**Na_2O**	−0.21	−1.13	**Na_2O**	−0.39	−2.09	**Na_2O**	−0.2	−1.09						
TiO_2	−0.32	−0.29															
		ppm															
Ba	−0.79	−2575.23	**Ba**	−0.68	−2226.9	**Ba**	−0.87	−2845.47	**Ba**	−0.83	−2718.31	**Ba**	−0.87	−2847.67	**Ba**	−0.87	−2853.08
Sr	−0.18	−162.12				**Sr**	−0.41	−369.88	**Sr**	−0.24	−212.17	**Sr**	−0.43	−383.65	**Sr**	−0.44	−390.21
Rb	−0.78	−102.25	**Rb**	−0.67	−87.58	**Rb**	−0.79	−103.85	**Rb**	−0.73	−95.57	**Rb**	−0.69	−91.01	**Rb**	−0.7	−91.53
V	−0.38	−61.44				**V**	−0.18	−29.46				**V**	−0.34	−55.13	**V**	−0.35	−56.5
Ce	−0.3	−26.26				**Ce**	−0.24	−21.16				**Ni**	−0.75	−31.52	**Ni**	−0.75	−31.65
La	−0.4	−20.72				**La**	−0.33	−17.11									
Nd	−0.28	−10.68										**Pb**	−0.8	−11.22	**Pb**	−0.8	−11.26
Y	−0.36	−6.13				**Pb**	−0.65	−9.23	**Pb**	−0.55	−7.78	**La**	−0.16	−8.54	**La**	−0.18	−9.09
Ga	−0.2	−4.34				**Ga**	−0.23	−4.84									
Cs	−0.78	−3.88				**Nd**	−0.18	−6.94									
Pr	−0.33	−3.49				**Y**	−0.17	−2.91									
			Cs	−0.66	−3.32	**Cs**	−0.57	−2.83				**Sc**	−0.21	−2.72	**Sc**	−0.22	−2.86

Table 3
Mass balance and Isocon calculations with constant Al_2O_3 content for the different sample with similar texture and location L4–L3 (smectite: lava flows); L2–L1 (chlorite/smectite mixed–layer: lava flows); Lt2–Lt1 (chlorite/smectite mixed–layer: lapilli tuff); Sr1–Sr2 (corrensite: lava flows) Located in Fig. 1C and D).

L4 → L3					L2 → L1					Lt2 → Lt1
Smec-altered lava			Δ volume = 4%		C/S altered lava			Δ volume = 8%		C/S altered lapilli tuff
Constant volume	$\Delta C_i/C_i^0$	ΔC_i	Δ mass = 4%					Δ mass = 7%		Constant volume
			Constant Al		Constant volume	$\Delta C_i/C_i^0$	ΔC_i	Constant Al		
			$\Delta C_i/C_i^0$	ΔC_i				$\Delta C_i/C_i^0$	ΔC_i	
Gain		%								
					LOI	0.5	3.23	0.63	4.01	**CaO**
					CaO	0.36	2.62	0.47	3.44	**LOI**
					$\%C_{TOTAL}$	3.45	1.49	3.82	1.64	$\%C_{TOTAL}$
					CO_2 equivalent		*5.5*			***CO_2 equivalent***
										K_2O
		ppm								
										Sr
					Zn	0.79	59.97	0.94	71.07	**Co**
					Cu	0.55	17.13	0.68	21.06	**Rb**
Ni	0.15	26.00	0.2	34.38	**Ni**	0.16	14.88	0.26	23.66	**Cu**
										Pb
Loss		%								
			Al2O3					**Al2O3**	**cst**	
K_2O	−0.16	−0.3	−0.12	−0.23	**Fe_2O_3**	−0.28	−2.35	−0.22	−1.86	**Na_2O**
					MgO	−0.27	−2.04	−0.21	−1.6	**Fe_2O_3**
		ppm								
					Ba	−0.49	−387.09	−0.45	−353.85	
Ba	−0.14	−113.00	−0.11	−84.5	**Sr**	−0.33	−248.44	−0.28	−207.21	**Ni**
					Pb	−0.84	−24.04	−0.82	−23.65	**V**
Cu	−0.16	−5.5	−0.13	−4.32	**Rb**	−0.24	−8.2	−0.17	−6.04	**Zn**
										Ga
										Y

L4 → L3			Lt2 → Lt1		Sr1 → Sr2					
Smec-altered lava			C/S altered lapilli tuff		Δ volume = −3%		Co altered lava			Δ volume = −0.2%	
Constant volume	$\Delta C_i/C_i^0$	ΔC_i	$\Delta C_i/C_i^0$	ΔC_i	Δ mass = −4%					Δ mass = −0.2%	
					Constant Al		Constant volume	$\Delta C_i/C_i^0$	ΔC_i	Constant Al	
					$\Delta C_i/C_i^0$	ΔC_i				$\Delta C_i/C_i^0$	ΔC_i
Gain		%									
			0.31	2.47	0.28	2.2					
			0.22	1.79	0.19	1.53					
			0.41	0.6	0.38	0.54	**LOI**	0.3	0.9	0.3	0.89
				2.21		*2.01*					
			0.24	0.41	0.21	0.35					
		ppm									
			0.43	230.63	0.39	210.78					
			5.63	147.49	5.46	142.99	**Sr**	0.17	70.9	0.16	70.07

(*continued on next page*)

Table 3 (*continued*)

L4 → L3			Lt2 → Lt1		Sr1 → Sr2							
Smec-altered lava			C/S altered lapilli tuff		Δ volume = −3%		Co altered lava			Δ volume = −0.2%		
Constant volume	$\Delta C_i/C_i^0$	ΔC_i	$\Delta C_i/C_i^0$	ΔC_i	Δ mass = −4%		Constant volume			Δ mass = −0.2%		
					Constant Al			$\Delta C_i/C_i^0$	ΔC_i	Constant Al		
					$\Delta C_i/C_i^0$	ΔC_i				$\Delta C_i/C_i^0$	ΔC_i	
			0.5	15.17	0.46	13.98	**Cu**	0.15	46.5	0.14	45.9	
Ni	0.15	26.00	0.28	7.5	0.24	6.6	**Rb**					
			0.84	6.44	0.79	6.07						
Loss		%										
					Al2O3	**cst**				**Al2O3**	**cst**	
K_2O	−0.16	−0.3	−0.29	−1.16	−0.31	−1.24						
			−0.14	−1.00	−0.16	−1.16						
		ppm										
Ba	−0.14	−113.00	−0.86	−135.46	−0.86	−136.05	**Zn**	−0.39	−90.00	−0.39	−90.23	
			−0.72	−78.15	−0.73	−78.92						
Cu	−0.16	−5.5	−0.7	−43.42	−0.71	−43.9						
			−0.72	−12.96	−0.72	−13.09						
			−0.21	−2.83	−0.23	−3.11	**Au**	−0.39	−2.8	−0.39	−2.81	

an unappropriated protolith considering the porosity of volcanoclastic rocks. Consequently, we selected as parent rock the less altered rock from the Seival area (Sr3 LOI: 1.9%). Consequently, mass balance changes from parent to daughter rocks do not represent magmatic to meteoric hydrothermal changes, but increasing degree of hydrothermal alteration. The less altered material from host phenocrysts of andesine–labradorite with albite (Sr3) and altered rocks have dominant smectite (smectite–rich C/S: L2 to L1; smectite and calcite: L4 to L3) or corrensite with minor calcite (Sr1 to Sr2). Like NAR, the use of Sr3 as parent rock gave an unrealistic volume and loss of material for lapilli tuff. Nevertheless, mass balance and Isocon calculations (Table 2; Supplementary material) of Sr3 parent rock with lava flows and subvolcanic rocks (Sr3 ➔ L4 and L3; Sr3 ➔ Sr1 and 2) show an apparent low–mobility of ~27 to 8% for SiO_2 compare to K_2O and Na_2O. These calculations suggest that Si and Al released during alteration were in situ entrapped, whereas the K_2O and Na_2O losses suggest a mobility or lixiviation by the alteration. The gains of C_{tot} and CaO are dominantly related to calcite deposition as attest the C_{tot} content equivalent CO_2 obtained with acid digestion of calcite. Whereas, LOI, Fe_2O_3 and MgO increases relate to changes associated with the formation of smectite, chlorite/smectite and corrensite and scarce iron oxides.

Trace elements gained are Cu, Zn, Ni, Ba, Rb, and Sr, with losses of some lanthanides for the increasing alteration. The Ce, La, Pb, Nd, and Ga seem particularly mobile for smectite–rich chlorite/smectite, whereas some Ce is gained for the corrensite and calcite alteration ($\Delta Ci/Ci^0$; supplementary material and Table 2). We interpret the REE loss as the consequence of fluid dilution (LOI) and the low– REE affinity of clay minerals (Yu et al., 2017). Nevertheless, the Ce enrichment noticed for corrensite and calcite suggest that fluid with pH modifying Ce concentrations (cf., Vaniman et al., 2002). These mass balance calculations looking at changes altered to very altered materials with Cu, Zn gains associated with precipitation of Fe–Mg–rich clays and calcite suggest an influx of aqueous or aqueous–carbonic fluid capable to transport base metals.

5.3. Mass balance calculations for materials with diverse textures and alteration intensity

The previous mass balances calculations provide information on large mineralogical changes with increasing clay minerals compare to albite content (Sr3). The following part attempt to compare rocks with an identical texture and increasing amounts of clay minerals (LOI: ca. 6 or 6 to 8; Table 3; Supplementary material).

The lava flows with smectite (L1 ➔ L2) or smectite–rich chlorite/smectite (L3 ➔ L4), lapilli tuff with chlorite/smectite mixed layers (Lt1 ➔ Lt2) and subvolcanic rocks (Sr1 ➔ Sr2) with albite and corrensite. The smaller changes in LOI between samples compared to previous calculations (5.2. Part) implies smaller $\Delta Ci/Ci^0$ changes. The minor volume and mass changes (−4 to +8%; Table 3) with increasing degree of alteration with gains of CaO, LOI, and C_{tot}, low–gains and losses K_2O, Ba and Zn, Cu, Sr, and Co. The gains related to the dominant precipitation of calcite (CaO, C_{tot}, LOI, Sr, Cu, Zn) with minor precipitation or dissolution of illite or oligoclase (K, Sr), sulfate (Ba, Sr), and sulfide (Cu, Zn, Co). Similar to volume changes from less–altered to more altered rocks, the increasing volume and mass of lava flows (+8%) indicate a precipitation of clay minerals and calcite precipitation with a volume expansion. Whereas, the decreasing volume (−3 to −4%) suggest a precipitation clay minerals and calcite filling the porosity in the lapilli tuff. The subvolcanic rocks with albite, corrensite, and no calcite show the smallest volume and mass changes (Table 3).

The small to no mass change concerning SiO_2 and Al_2O_3 indicate that increasing amount of clay minerals are related to in situ alterations of silicate in lava flows (L) and lapilli tuff (Lt), and subvolcanic rocks (Sr). The addition of 'external' Ca, and LOI relates to aqueous carbonic fluids with the crystallization of calcite in L and Lt, but the loss of Fe_2O_3, MgO > Ba, Sr or Na_2O, and Fe_2O_3 > Y. We interpreted this loss as a leaching by reducing fluid with low pH or partial pressure of oxygen (Lottermoser, 1992; Lewis et al., 1998; Williams-Jones et al., 2012). In subvolcanic rocks gained

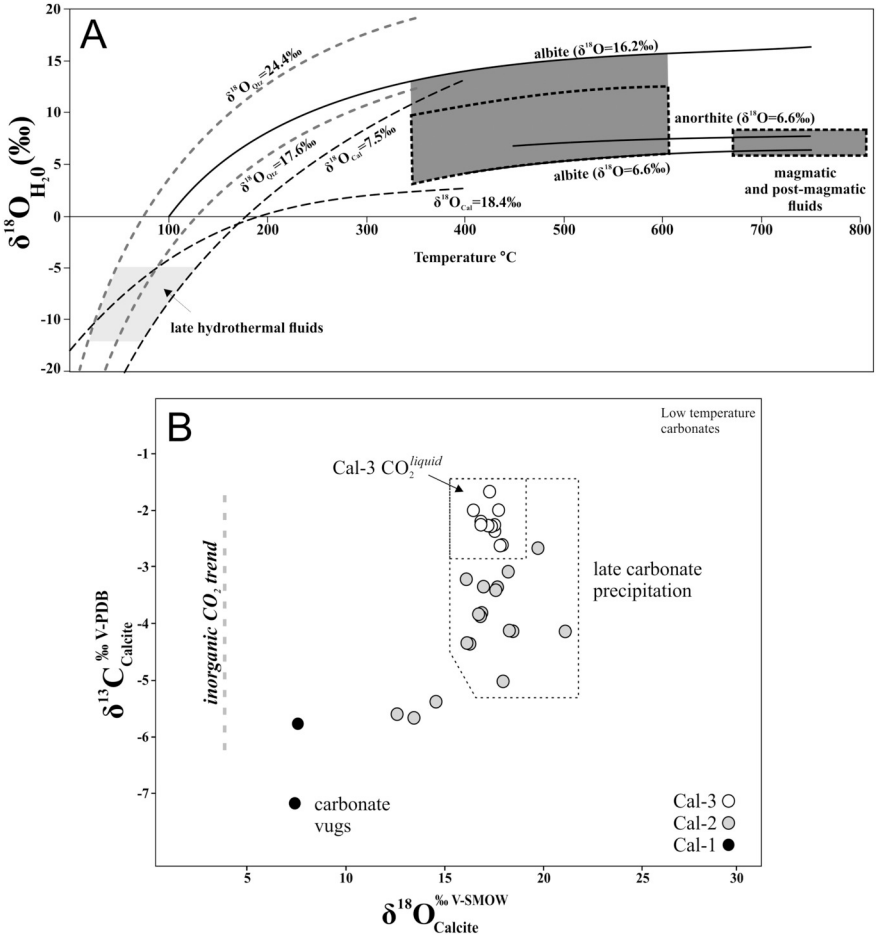

Fig. 4. A) Temperature vs. calculated $\delta^{18}O_{H2O}$ (‰ V–SMOW) values (Zheng, 1993) from andesine–labradorite, albite–rich plagioclases, calcite (vesicles and veins) and euhedral quartz (Fig. 2C and D); B) $\delta^{18}O$ from calcite 1 to 3 (‰ V–SMOW) vs. $\delta^{13}C$ (‰ V–PDB) obtained in calcite veins (Cal–2 and –3) and vesicles (Cal–1) (Fig. 2 and Table 1).

LOI, Sr, Cu (several hundreds of ppm), and losses of Zn and Au (Tables 2 and 3) suggest that fluids associated with corrensite were chemically or chronologically different than in lava flows and lapilli tuff.

The in–situ source of metals is suggested by the concentration of Si which present $\Delta Ci/Ci^0$ ca. 0 to 2; (Tables 2 and 3; Supplementary material) and Al constant is reinforced REE by low mobility or REE– immobility ($\Delta Ci/Ci^0$). Excepted for Cs, Gd, and Eu for chlorite/smectite– calcite and corrensite, the immobility of REE indicates that external aqueous or aqueous–carbonic water precipitating clay minerals and calcite had a minor influence on the REE total concentrations of the different rocks. Consequently, we interpreted major element and REE chemical changes with increasing degree of alteration as products of the in–situ transformation of volcanic rocks.

The different steps of alteration by albite, clay minerals to calcite (Part 5.2) a metallic enrichment not associated with increasing alteration (Part 5.3), except for subvolcanic rocks with corrensite indicate metal and base metal enrichments seem derived from lixiviation of surrounding lava flows and volcanoclastic rocks, and fluid/rock interaction associated with albitization and corrensite formation. The following part will attempt to identify the magmatic, late–magmatic or late meteoric origin of fluids involved in these fluid/rock interactions.

5.4. High–temperature magmatic and late–magmatic fluids

The andesine–labradorite phenocrysts indicate a magmatic crystallization with equilibrium temperature going from 800 to 500 °C (Gill, 1981; Devine, 1995; Blundy et al., 2006). The albitization is described late–magmatic or subsolidus recrystallization between 600 and 350 °C (cf., Huang et al., 2009; Hövelmann et al., 2010), and smectite, chlorite/smectite at a lower temperature. In the Seival area, lack of kaolinite or iron oxides caprock suggest that the lower temperatures were higher than supergene (> 50 °C) and bracketed by low–temperature of albitization (< 350 °C). Assuming magmatic temperature (800 to 600 °C, reference therein) for andesine–oligoclase formation then calculated $\delta^{18}O$ magmatic fluids ($\delta^{18}O_{H2O}$) in equilibrium vary from 5.3 to 6.7‰ (oxygen fractionation factor; Zheng, 1993). The preservation of andesine–labradorite phenocrysts and calculated $\delta^{18}O_{H2O\ melt}$ values for andesine–labradorite do not indicate primary magmatic fluid (Sheppard, 1986), but a mixture of magmatic and meteoric or fluid/rock evolved magmatic fluids (Bongiolo et al., 2011). We calculated $\delta^{18}O_{H2O}$ values of fluids in equilibrium with albite–rich plagioclase formed between 600 and 350 °C (Zheng, 1993) vary from12 to 10‰ (Fig. 4A). The $\delta^{18}O_{H2O}$ values of albite compared to $\delta^{18}O_{H2O}$ of andesine–labradorite suggests an albitization associated with an evolved magmatic fluid (Table 4). This ^{18}O enrichment cannot be related to meteoric fluids but could be due to oxygen isotope exchange of CO_2–H_2O or CO_2–calcite (Bottinga and Craig, 1968; Bottinga and Javoy, 1989) or increasing fluid/rock ratio (Taylor Jr., 1974; Pollard, 2001; Goll et al., 2003). The occurrence of small aqueous–carbonic fluid inclusions observed in calcite vein (Fontana et al., 2017) attests of magmatic CO_2, but do not certainly relate it to albite formation (Perez and Boles, 2005). This stable isotope interpretation confirms that albitization with Na–rich fluid was related to late–magmatic related to cooling or degassing lava flows with aqueous and CO_2–rich fluid rather than high–temperature meteoric water.

Table 4
$\delta^{18}O$, $\delta^{13}C$ values reported as per mil (‰) relative to V–SMOW and V–PDB for calcite, quartz, altered pyroxene, andesine–labradorite, and albite–rich separates.

Location ID	Depth (m)	Sample type	$\delta^{18}O$ ‰	$\delta^{13}C$ ‰	$\delta^{18}O$ ‰
			Qtz *; Pl; Px**	Calcite	Calcite
1	*Surface*	*Vein(Cal-3)*		−2.25	17.5
1	*Surface*	*Vein(Cal-3)*			
2	*Surface*	*Not alterd Pl.*	6.6; 6.8		
3	*Surface*				
3	*Surface*				
3	*Surface*				
4	*Surface*	*Vein(Cal-3)*	13.75	−1.65	17.34
5	*60*	*Vein(Cal-3)*		−3.2	16.16
5	*Surface*		16.1	−3.33	17.03
5	*Surface*	*Vein(Cal-3)*			
4	*Surface*	*Not alterd Pl.*	6.7; 7.9; 8.1		
7	*Surface*	*Vein(Cal-3)*		−3.27	17.59
7	*Surface*	*Vein(Cal-3)*		−1.98	17.79
7	*Surface*	*Vein(Cal-3)*		−2.1; −2.2; −2.5	16.8; 17.3; 17.9
7	*Surface*				
7	*Surface*				
7	*Surface*				
7	*Surface*				
8	*Surface*				
9	*14*	*Vein(Cal-2)*		−5.37	14.62
9	*14*	*Vesicles(Cal-1)*		−7.16; −5.7	7.48; 7.63
10	*15*	*Vein(Cal-2)*	* 19.2; 19.9; 20.4; 20.9; 24.4		
11	*41*	*altered Pl.*	14.8; 14.8; 14.9		
12	*43*	*altered Pl.*	15.1; 15.4		
13	*50*	*Vein(Cal-2)*		−5.59	12.65
14	*37*	*altered Pl.*	15.6; 15.7		
15	*40*	*altered Pl.*	15.5; 16.2		
16	*119*	*Vein(Cal-2)*	* 17.6		
17	*15*	*Vein(Cal-3)*	* 20.2		
18	*22*	*Vein(Cal-3)*	* 19.7; 21; 21; 20.2		
18	*22*			−4.0; −4.1	18.3; 18.4
19	*22*	*Vein(Cal-3)*		−4.24	16.24
2	*Surface*	*Px-01*	10,3**		
2	*Surface*	*Clays from PX1*	23.80		
2	*Surface*	*Calcite in PX1*		−3.40	17.6
2	*Surface*	*Px-02*	8,6**		
2	*Surface*	*Clays from PX2*	27.60		
2	*Surface*	*Calcite in Px2*		−3.45	17.7
2	*Surface*	*Px-03*	8,5**		
2	*Surface*	*Clays from PX3*	26.60		
2	*Surface*	*Px-04*	10,7**		

5.5. Stable isotope values of aqueous and aqueous carbonic fluids

Pyroxene altered to chlorite shows oxygen isotope with intermediate values, between magmatic pyroxene ($\delta^{18}O_{Px}$ ca. 5‰; cf., Eiler, 2001; Hoefs, 2004; Sharp, 2006) and the $\delta^{18}O$ values of clay minerals (23 to 28‰). Considering a binary mixture, we calculated the proportion of clay minerals in altered pyroxene. The proportions of clay minerals vary between 20 and 40% in agreement with petrographic observation.

We combined the oxygen fractionation factor of chlorite and smectite for temperature between 50 and 200 °C (eg., Kloprogge, 1999; Kameda et al., 2011) with $\delta^{18}O$ values of chlorite/smectite in pyroxene phenocrysts. The $\delta\ ^{18}O_{\ chlorite-\ H2O}$ and $\delta\ ^{18}O_{\ smectite-\ H2O}$ vary from 10.3‰ to 2.3‰ and 17.2 to 5.7‰ at 50 and 200 °C, respectively (chlorite: Wenner, 1971 or chlorite and smectite: Savin and Lee, 1988). The calculated $\delta\ ^{18}O_{H2O}$ indicate unrealistic positive values (> 10‰) suggesting a wrong assumption related to the temperature range or mineralogy. Further study of altered pyroxene should be considered.

The petrography with different albite, clay minerals, quartz, and calcite precipitation (Cal–1 to 3; cf. Fontana et al., 2017), the gain of calcium, carbon, and with aqueous–carbonic fluid inclusions (Fontana et al., 2017) suggest that some fluids may derive from magma degassing (Craig, 1953; Belkin et al., 1985; Chacko et al., 2001) or meteoric water and organic matter interaction (Cerling and Quade, 1993). The different $\delta^{13}C_{Cal}$ values from calcite in vesicles (−7.1‰; Cal–1) and calcite veins (−5.5 to −1.7‰; Cal–2 and 3) are similar those measured in the large epithermal deposit of Minas do Camaquã (Renac et al., 2014). The $\delta^{13}C_{Cal\ values}$ confirm a dominant source of inorganic carbon (reference therein; Fig. 4B) rather than organic matter. These negative to less negative trends of $\delta^{13}C_{Cal}$ values, from vesicle (Cal–1) to veins (Cal–2 and 3) occur in modern volcanoes with mixtures of carbon from CO_2 volcanic and CO_2 air (e.g., Chiodini et al., 2011). The changes of $\delta^{18}O_{Cal}$ values from 7.5 (vesicle, Cal–1) to 18.4 and 12‰ (veins or pyroxene; Cal–2 and 3) indicate either variation of temperature or $\delta^{18}O_{H2O}$ value of fluid.

We bracketed the temperature of calcite precipitation between albitization (< 350 °C) and supergene alteration (50 °C). Nevertheless, the precipitation of calcite occurs with smectite, chlorite/smectite, and corrensite. Consequently, we restrained the temperature formation between 250 and 50 °C between the field of stability of chlorite (Meunier et al., 1988; Kameda et al., 2011) and smectite (Kloprogge, 1999). This temperature range allows calculation of $\delta^{18}O_{H2O}$ values (Fig. 4) in equilibrium with calcite (oxygen fractionation factor: Kim and O'Neil, 1997) and euhedral quartz (oxygen fractionation factor: Clayton et al., 1972) from veins with calcite (Cal–3). The calculated $\delta^{18}O_{H2O}$ values vary from −12 to 0‰ for calcite, −12 to −5‰ for quartz and a quartz sample with a $\delta^{18}O_{H2O}$ of +5‰. The majority of calculated $\delta^{18}O_{H2O}$ values indicate meteoric fluids (−12 to 0‰), similar to the intense argillic alteration (−1.6 to +1.8‰), and the

volcanic propylitic alteration (−12 to −10‰) in the Hilário Formation and the Lavras do Sul granite (Bongiolo et al., 2011). The positive $\delta^{18}O_{H2O}$ values for a quartz precipitation suggest a local contribution magmatic water (+5‰).

The proximity of Lavras do Sul granite and the similar range of calculated $\delta^{18}O_{H2O}$ values for quartz and calcite suggest that hydrothermal alterations are related to a large epithermal system (Fig. 1). The $\delta^{18}O_{H2O}$ values of meteoric suggest cold rainfall ($\delta^{18}O_{H2O}$: −12‰) to coastal water (0‰) or fluids similar to intense argillic alteration in the granite (Bongiolo et al., 2011). The influence of meteoric–hydrothermal recharge ($\delta^{18}O_{H2O}$) and a dominant inorganic source of carbon ($\delta^{13}C_{Cal}$) indicate that aqueous–carbonic fluids flowing in the Seival area are associated with the degassing of magmatic bodies. The magmatic bodies in the Seival area are the intrusive or intercalated andesitic–dikes, the Lavras do Sul Intrusive Complex emplaced during the Ediacaran time (Philipp et al., 2003, 2016) or a deeper source drained by faults of the area (Fig. 1). The mixture of meteoric water and degassing magma (aqueous carbonic fluid) is not favorable for base metal mobility (Part 5.3). Consequently, we suggest that the ore deposition in Seival area relates to late–magmatic fluid, albitization, and chloritization.

6. Conclusions

The study of mineralogical compositions, mass balance and O-C stable isotope calculations in the volcanic rocks from Seival Mine have allowed a better comprehension of base metal enrichment in this kind of copper mineralization.

In Seival area the hydrothermal alteration is controlled by volcanic lithotypes and structures associated with the fluid activity. The main mineral assemblage is magmatic plagioclase; followed by late-hydrothermal albite; Fe-Mg clays; quartz in veins and crystallization of three generations of carbonates filling fractures and vesicles. Mass balance results for andesitic rocks with decreasing intensity of hydrothermal alteration indicate short distance chemical variations (Si, Al, Fe, and Mg) associated with different textures (lava flows, lapilli tuff and subvolcanic rocks), except for Ca, C, and H_2O. The higher temperature fluid/rock interaction occurred with predominantly magmatic fluids associated with albitization or high–temperature chloritization processes. The calcite, smectite, chlorite/smectite, and corrensite are precipitated in a similar range of temperature. Chemical changes marked by loss of metal elements associated with corrensite are restricted to subvolcanic rocks. These clay minerals precipitations indicate volume expansion and decreasing volume linked to calcite filling porosity. Mass balance calculations indicate that hydrothermal alteration with chlorite/smectite and calcite did not mobilize Fe and Mg neither caused other gains of base metals.

The combination of mass balance and stable isotope interpretation indicates that metal enrichment was due early magmatic fluids ($\delta^{18}O_{H2O}$: +5‰) and the late–magmatic (or evolved magmatic fluids: +10‰) from 600 to 350 °C. The evolved magmatic fluids ($\delta^{18}O_{H2O}$: +10‰) indicate an ^{18}O enrichment during albite formation. The enrichment might be related to residual magmatic fluid (late–magmatic fluids) and CO_2–H_2O with lava flows out-gassing or CO_2– H_2O with calcite precipitation. The calcite precipitation with carbon and calcium gains, increasing volume (mass balance) is linked to the incursion of meteoric fluids (250 to 50 °C). Moreover, $\delta^{13}C_{values}$ of calcite $_{veins}$ of $\delta^{18}O_{H2O}$ of quartz and calcite indicate an inorganic source of carbon either related to outgassing lava or atmospheric CO_2 mixed with meteoric water (250 to 50 °C). Consequently, we propose that base metal enrichment is related to the lixiviation of surrounding lava flows and volcanoclastic rocks by late–magmatic fluids. The Cu and Ag–rich fluids were entrapped in the porous or driven through a network of fractures and intrusive dikes.

Acknowledgments

This study was partly funded by “Conselho Nacional de Desenvolvimento Cientifico e Tecnologico – CNPq” and CAPES-COFECUB (project n°619/08) and a personal grant to C. Renac from UNICE/GEOAZUR. The authors thank VOTORANTIM metal company for drillcore samples. Michel Manetti (in memoriam) for his help during the sampling strategy steps of this work.

Appendix A. Supplementary data

Supplementary data to this article can be found online at https://doi.org/10.1016/j.gexplo.2018.10.001.

References

Barrett, T.J., MacLean, W.H., 1999. Volcanic sequences, lithogeochemistry, and hydrothermal alteration in some bimodal volcanic–associated massive sulfide systems. In: Barrie, C.T., Hannington, M.D. (Eds.), Volcanic–Associated Massive Sulfide Deposits: Processes and Examples in Modern and Ancient Environments. Reviews in Economic Geology. Vol. 8. pp. 101–131.

Belkin, H., De Vivo, B., Gianelli, G., Lattanzi, P., 1985. Fluid inclusions in minerals from the geothermal fields of Tuscany, Italy. Geothermics 14 (1), 59–72.

Blundy, J., Cashman, K.V., Humphreys, M., 2006. Magma heating by decompression – driven crystallization beneath andesite volcanoes. Nature 443, 76–80.

Bongiolo, E.M., Renac, C., Mexias, A.S., Gomes, M.E.B., Ronchi, L.H., Patrier-Mase, P., 2011. Evidence of Ediacaran glaciation in southernmost Brazil through magmatic to meteoric fluid circulation in the porphyry–epithermal Au–Cu deposits of Lavras do Sul. Precambrian Res. 189, 404–419.

Bottinga, Y., Craig, H., 1968. High temperature liquid vapor fractionation factors for H_2O-HDO-$H_2{}^{18}0$. Eos 49, 356–357.

Bottinga, Y., Javoy, M., 1989. MORD degassing: Evolution of CO_2. Earth Planet. Sci. Lett. 95, 215–225.

Capuano, R.M., 1992. The temperature dependence of hydrogen isotope fractionation between clay minerals and water: evidence of a geopressured system. Geochim. Cosmochim. Acta 56, 2547–2554.

Cerling, T.E., Quade, J., 1993. Stable carbon and oxygen isotopes in soil carbonates. Climate change in continental isotopic records. Geophys. Monogr. 78, 217–231.

Chacko, T., Cole, D.R., Horita, J., 2001. Equilibrium oxygen, hydrogen and carbon isotope fractionation factors applicable to geologic systems. Rev. Mineral. Geochem. 43, 1–81.

Chemale Jr., F., 2000. Evolução Geológica do Escudo Sul–rio–grandense. In: Holz, M., De Ros, L.F. (Eds.), Geologia do Rio Grande do Sul. Ed. da Universidade/UFRGS, Porto Alegre, pp. 13–52.

Chemale Jr., F., Hartmann, L.A., da Silva, L.C., 1995. Stratigraphy and tectonism of Brasiliano Cycle in southern Brazil. Commun. Geol. Surv. Namibia 10, 151–166.

Chiodini, G., Caliro, S., Aiuppa, A., Avino, R., Granieri, D., Moretti, R., Parello, F., 2011. First $^{13}C/^{12}C$ isotopic characterization of volcanic plume CO_2. Bull. Volcanol. 73, 531–542.

Clayton, R.N., Mayeda, T.K., 1963. The use of bromine pentafluoride in the extraction of oxygen from oxides and silicates for isotopic analysis. Geochim. Cosmochim. Acta 27, 43–52.

Clayton, R.N., O'Neil, J.R., Mayeda, T.K., 1972. Oxygen isotope exchange between quartz and water. J. Geophys. Res. 77, 3057–3067.

Craig, H., 1953. The geochemistry of the stable carbon isotopes. Geochim. Cosmochim. Acta 3, 53–92.

Cruz, N., Peng, Y., Wightman, E., 2015. Interactions of clay minerals in copper–gold flotation: part 2–Influence of some calcium–bearing gangue minerals on the rheological behaviour. Int. J. Miner. Process. 141, 51–60.

De Caritat, P., Hutcheon, I., Walshe, J.L., 1993. Chlorite geothermometry: a review. Clay Clay Miner. 41 (2), 219–239.

Devine, J.D., 1995. Petrogenesis of the basalt – andesite dacite association of Grenada, Lesser Antilles island arc, revisited. J. Volcanol. Geotherm. Res. 69, 1–33.

Eiler, J.M., 2001. Oxygen isotope variations of basaltic lavas and upper mantle rocks. Rev. Mineral. Geochem. 43 (1), 319–364.

Fontana, E., Mexias, A.S., Renac, C., Nardi, L.V.S., Lopes, R.W., Barats, A., Gomes, M.E.B., 2017. Hydrothermal alteration of volcanic rocks in Seival Mine Cu–mineralization – Camaquã Basin – Brazil (part I): Chloritization process and geochemical dispersion in alteration halos. J. Geochem. Explor. 177, 45–60.

Gastal, M.C.P., Lafon, J.M., 2006. Multiple magma batches in the construction of the granite pluton, Lavras do Sul intrusive complex, southern Brazil: Sr-Nd isotopic and geochemical evidences. In: V South American Symposium on Isotope Geology, 2006, Punta del Este. Short Papers, pp. 370–374.

Gastal, M.C., Ferreira, F.J.F., da Cunha, J.U., Esmeris, C., Koester, E., Raposo, M.I.B., Rossetti, M.M.M., 2015. Alojamento do granito Lavras e a mineralização aurífera durante evolução de centro vulcano–plutônico pós–colisional, oeste do Escudo Sul–riograndense: Dados geofísicos e estruturais. Braz. J. Geol. 45, 217–241.

Gill, J.B., 1981. Orogenic Andesites and Plate Tectonics, first ed. Springer–Verlag, Berlin Heidelberg (390 pp).

Goll, M., Lippolt, H.J., Hoefs, J., 2003. (Thüringer Wald, Germany): Ar, Sr and O isotope evidence. Chem. Geol. 199, 209–231.

Grant, J.A., 1986. The isocon diagram–a simple solution to Gresens equation for metasomatic alteration. Econ. Geol. 81, 1976–1982.

Gresens, R.L., 1967. Composition–volume relationships of metasomatism. Chem. Geol. 2, 47–55.

Hallinan, S.E., Mantovani, M.S.M., Shukowski, W., Braggion Jr., I., 1993. Estrutura do Escudo Sul–brasileiro: uma revisão através de dados gravimétricos e magnetométricos. Braz. J. Geol. 23, 201–214.

Hartmann, L.A., Philipp, R.P., Santos, J.O.S., McNaughton, N.J., 2011. Time frame of 753–680 Ma juvenile accretion during the São Gabriel orogeny, southern Brazillian Shield. Gondwana Res. 19, 84–99.
Henley, R.W., 1985. The geothermal framework of epithermal deposits. In: BERGER, B.R., Bethke, P.M. (Eds.), Geology and Geochemistry of Epithermal Systems. Reviews in Economic Geology. Vol. 2. pp. 1–24.
Hoefs, J., 2004. Stable Isotope Geochemistry.
Hövelmann, J., Putnis, A., Geisler, T., Schmidt, B.C., Golla-Schindler, U., 2010. The replacement of plagioclase feldspars by albite: observations from hydrothermal experiments. Contrib. Mineral. Petrol. 159, 43–59.
Huang, F., Lundstrom, C.C., Glessner, J., Ianno, A., Boudreau, A., Lia, J., Ferré, E.C., Marshak, S., DeFrates, J., 2009. Chemical and isotopic fractionation of wet andesite in a temperature gradient: experiments and models suggesting a new mechanism of magma differentiation. Geochim. Cosmochim. Acta 73, 729–749.
Huston, D.L., 1993. The effect of alteration and metamorphism on wall rocks to the Balcooma and Dry River South volcanic–hosted massive sulfide deposits, Queensland, Australia. J. Geochem. Explor. 48, 277–307.
Ishikawa, Y., Sawaguchi, T., Ywaya, S., Horiuchi, M., 1976. Delineation of prospecting targets for Kuroko deposits based on modes of volcanism of underlying dacite and alteration haloes. Min. Geol. 26, 105–117.
Jiang, W.T., Peacor, D.R., Buseck, P.R., 1994. Chlorite geothermometry – Contamination and apparent octahedral vacancies. Clay Clay Miner. 42, 593–605.
Kameda, J., Ujiie, K., Yamaguchi, A., Kimura, G., 2011. Smectite to chlorite conversion by frictional heating along a subduction–zone thrust. Earth Planet. Sci. Lett. 305, 161–170.
Kaur, P., Chaudhri, N., Hofmann, A., Raczek, I., Okrusch, M., Skora, S., 2012. Two–Stage, extreme albitization of A–type granites from Rajasthan, NW India. J. Petrol. 53, 919–948.
Kim, S.T., O'Neil, J.R., 1997. Equilibrium and nonequilibrium oxygen isotope effects in synthetic carbonates. Geochim. Cosmochim. Acta 61, 3461–3475.
Kloprogge, J.T., 1999. Synthesis of Smectite Clay Minerals: a critical Review. Clay Clay Miner. 47, 529–554.
Large, R.R., Gemmell, J.B., Paulick, H., Huston, D.L., 2001. The alteration box plot: a simple approach to understanding the relationship between alteration mineralogy and lithogeochemistry associated with volcanic–hosted massive sulphide deposits. Econ. Geol. 96, 957–971.
Lewis, A.J., Komninou, A., Yardley, B.W.D., Palmer, M.R., 1998. Rare earth element speciation in geothermal fluids from Yellowstone National Park, Wyoming, USA. Geochim. Cosmochim. Acta 62 (4), 657–663.
Lima, E.F., 1995. Petrologia das Rochas Vulcânicas e Hipoabissais da Associação Shoshonítica de Lavras do Sul – ASLS, RS (Doctoral Thesis). IGc–UFRGS, Porto Alegre (338 pp).
Lima, E.F., Nardi, L.V.S., 1992. O magmatismo shoshonítico no estado do Rio Grande do Sul. Uma revisão. Pesquisas em Geociências 19, 190–194.
Lima, E.F., Nardi, L.V.S., 1998. The Lavras do Sul shoshonitic association: implications for origin and evolution of Neoproterozoic shoshonitic magmatism in southernmost Brazil. J. S. Am. Earth Sci. 11, 67–77.
Liz, J.D., Lima, E.F., Nardi, L.V.S., 2008. Avaliação de fontes magmáticas de series shoshoníticas pós–colisionais com base na normalização pela Associação Shoshonítica de Lavras do Sul – aplicação de Sliding Normalization. Braz. J. Geol. 39, 55–66.
Lopes, R.W., Fontana, E., Mexias, A.S., Gomes, M.E.B., Nardi, L.V.S., Renac, C., 2014. Caracterização petrográfica e geoquímica da sequência magmática da Mina do Seival, Formação Hilário (Bacia do Camaquã – Neoproterozóico), Rio Grande do Sul, Brasil. Revista Pesquisas em Geociências 41, 51–64.
López-Moro, F.J., 2012. EASYGRESGRANT–A Microsoft Excel spreadsheet to quantify volume changes and to perform mass–balance modeling in metasomatic systems. In: Computers & Geosciences. Vol. 39. pp. 191–196.
Lottermoser, B.G., 1992. Rare earth elements and hydrothermal ore formation processes. Ore Geol. Rev. 7 (1), 25–41.
MacLean, W.H., 1990. Mass change calculations in altered rock series. Mineral. Deposita 25, 44–49.
McCrea, J.M., 1950. On the isotopic chemistry of carbonates and a paleotemperature scale. J. Chem. Phys. 18, 849–857.
Meunier, A., Clement, J.Y., Bouchet, A., Beaufort, D., 1988. Chlorite–calcite and corrensite–dolomite crystallization during two superimposed events of hydrothermal alteration in the "Les Cretes" Granite, Vosges, France. Can. Mineral. 26, 413–442.
Mexias, A.S., Formoso, M.L.L., Meunier, A., Beaufort, D., 1990. Composition and crystallization of corrensite in volcanic and pyroclastic rocks of Hilário Formation (RS) Brazil. Sci. Géol. 88, 135–143.
Mexias, A.S., Bongiolo, E.M., Gomes, M.E.B., Formoso, M.L.L., Frantz, J.C., 2007. Alterações hidrotermais e mineralizações nas rochas da Associação Plutono–Vulcano–Sedimentar da região de Lavras do Sul–RS. In: Ianuzzi, R., Frantz, J.C. (Eds.), 50 Anos de Geologia: Instituto de Geologia, Contribuições. Ed. Comunicação e Identidade, Porto Alegre, pp. 143–159.
Nardi, L.V.S., Lima, E.F., 1985. A Associação Shoshonítica de Lavras do Sul, RS. Braz. J. Geol. 15, 139–146.
Nardi, L.V.S., Lima, E.F., 1988. Hidrotermalismo no complexo granítico Lavras e vulcânicas associadas, RS. Braz. J. Geol. 18, 369–375.
Paim, P.S.G., Chemale Jr., F., Lopes, R.C., 2000. A Bacia do Camaquã. In: Holz, M., De Ros, L.F. (Eds.), Geologia do Rio Grande do, Sul. Ed. Da Universidade/UFRGS, Porto Alegre, pp. 231–374.
Pearce, T.H., 1968. A contribution to the theory of variation diagrams. Contrib. Mineral. Petrol. 19, 142–157.
Pearce, T.H., 1987. The identification and assessment of spurious trends in Pearce–type ratio variation diagrams: a discussion of some statistical arguments. Contrib. Mineral. Petrol. 97, 529–534.
Perez, R.J., Boles, J.R., 2005. An empirically derived kinetic model for albitization of detrital plagioclase. Am. J. Sci. 305 (4), 312–343.
Philipp, R.P., Machado, R., Chemale Jr., F., 2003. Reavaliação e Novos Dados Geocronológicos (Ar/Ar, Rb/Sr e Sm/Nd) do Batólito Pelotas no Rio Grande do Sul: Implicações Petrogenéticas e Idade de Reativação das Zonas de Cisalhamento. Revista Geologia USP 3, 71–84.
Philipp, R.P., Machado, R., Chemale Jr., F., 2007. A geração dos granitóides Neoproterozóicos do Batólito Pelotas: evidências dos isótopos de Sr e Nd e implicações para o crescimento continental da porção sul do Brasil. In: Iannuzzi, R., Frantz, J.C. (Eds.), 50 anos de Geologia: Instituto de Geociências. Contribuições. Comunicação e Identidade, Porto Alegre, pp. 59–77.
Philipp, R.P., Pimentel, M.M., Chemale Jr., F., 2016. Tectonic evolution of the Dom Feliciano Belt in Southern Brazil: Geological relationships and U–Pb geochronology. Braz. J. Geol. 46, 83–104.
Pollard, P.J., 2001. Sodic (−calcic) alteration in Fe–oxide–Cu–Au districts: an origin via unmixing of magmatic H_2O–CO_2–NaCl ± $CaCl_2$–KCl fluids. Mineral. Deposita 36 (1), 93–100.
Raposo, M.I.B., Gastal, M.C.P., 2009. Emplacement mechanism of the main granite pluton of the Lavras do Sul intrusive complex, South Brazil, determined by magnetic anisotropies. Tectonophysics 466, 18–31.
Reischl, J.L., 1978. Mineralizações cupríferas associadas a vulcânicas na Mina do Seival. In: Anais do XXX Congresso Brasileiro de Geologia, Recife, pp. 1568–1582.
Remus, M.V.D., McNaughton, N.J., Hartmann, L.A., Groves, D.I., 1997. Pb and S isotope signature of sulfides and constraints on timing and sources of Cu (Au) mineralization at the Camaquã and Santa Maria Mine, Caçapava do Sul, southern Brazil. In: South American Symposium Isotopic Geology. SSAGI, São Paulo, pp. 253–255.
Remus, M.V.D., Hartmann, L.A., McNaughton, N.J., Groves, D.I., Reischl, J.L., 2000. A distal magmatic–hydrothermal origin for the Camaquã Cu (Au–Ag) and Santa Maria Pb, Zn (Cu–Ag) deposits, southern Brazil. Gondwana Res. 3, 155–174.
Renac, C., Mexias, A.S., Gomes, M.E.B., Ronchi, L.H., Nardi, L.V.S., Laux, J.H., 2014. Isotopic fluid changes in a Neoproterozoic porphyry epithermal system: the Uruguay mine, southern Brazil. Ore Geol. Rev. 60, 146–160.
Saalmann, K., Hartmann, L.A., Remus, M.V.D., Koester, E., Conceição, R.V., 2005. Sm–Nd isotope geochemistry of metamorphic volcano–sedimentary successions in the São Gabriel Block, southernmost Brazil: evidence for the existence of juvenile Neoproterozoic oceanic crust to the east of the Rio de la Plata craton. Precambrian Res. 136, 159–175.
Saalmann, K., Hartmann, L.A., Remus, M.V.D., 2007. The assembly of West Gondwana–The view from the Rio de la Plata craton. In: Linnemann, U., Nance, R.D., Kraft, P., Zulauf, G. (Eds.), The Evolution of the Rheic Ocean: From Avalonian–Cadomian Active Margin to Alleghenian–Variscan Collision. Geological Society of America Special Paper. Vol. 423. pp. 1–26.
Saalmann, K., Gerdes, A., Lahaye, Y., Hartmann, L.A., Remus, M.V.D., 2011. A multiple accretion at the eastern margin of the Rio de la Plata craton: the prolonged Brasiliano orogeny in southernmost Brazil. Int. J. Earth Sci. 100, 355–378.
Savin, S.M., Lee, M., 1988. Isotopic studies of phyllosilicates. In: Bailey, S.W. (Ed.), Hydrous Phyllosilicates. Reviews in Mineralogy Vol. 19. Mineralogical Society of America, Washington, D.C, pp. 189–223.
Schleicher, A.M., van der Pluijm, B.A., Warr, L.N., 2012. Chlorite–smectite clay minerals and fault behavior: New evidence from the San Andreas Fault Observatory at Depth (SAFOD) core. Lithosphere 4, 209–220.
Sharp, Z., 2006. Principles of Stable Isotope Geochemistry. Prentice Hall.
Sheppard, S.M.F., 1986. Characterization and isotopic variations in natural waters. In: Valley, J.W., Taylor Jr.H.P., O'Neil, J.R. (Eds.), Stable Isotopes in High–Temperature Geological Processes. Reviews in Mineralogy and Geochemistry Vol. 16. pp. 165–183.
Sillitoe, R.H., 2010. Porphyry Copper Systems. Econ. Geol. 105, 3–41.
Stanley, C.R., Madeisky, H.E., 1994. Lithogeochemical exploration for hydrothermal ore deposits using Pearce element ratio analysis. In: Lentz, D. (Ed.), Alteration and Alteration Processes Associated With Ore Forming Systems. Geological Association of Canada Short Course Notes Vol. 11. pp. 193–211.
Tardy, Y., Duplay, J., Fritz, B., 1987. Stability Fields of Smectites and Illites as a Function of Temperature and Chemical Composition.
Taylor Jr., H.P., 1974. An application of oxygen and hydrogen isotope studies to problems of hydrothermal alteration and ore deposition. Econ. Geol. 69, 843–883.
Vaniman, D.T., Chipera, S.J., Bish, D.L., Duff, M.C., Hunter, D.B., 2002. Crystal chemistry of clay–Mn oxide associations in soils, fractures, and matrix of the Bandelier Tuff, Pajarito Mesa, New Mexico. Geochim. Cosmochim. Acta 66 (8), 1349–1374.
Vaughan, D.J., Corkhill, C.L., 2017. Mineralogy of Sulfides. Elements 13 (2), 81–87.
Veigel, R., Dardena, M.A., 1990. Paragênese e sucessão mineral nas diferentes etapas da evolução da mineralização Cu–Pb–Zn do Distrito de Camaquã, RS. Braz, J. Geol. 20, 55–67.
Wenner, D.B., 1971. Hydrogen and Oxygen Isotopic Studies of Serpentinization of Ultramafic Rocks (Ph.D. Thesis). California Institute of Technology.
Wildner, W., Lima, E.F., Nardi, L.V.S., Sommer, C.A., 2002. Volcanic cycles and setting in the Neoproterozoic III to Ordovician Camaquã Basin succession in southern Brazil: characteristic of post–collisional magmatism. J. Volcanol. Geotherm. Res. 118, 261–283.
Williams-Jones, A.E., Migdisov, A.A., Samson, I.M., 2012. Hydrothermal mobilisation of the rare earth elements–a tale of "ceria" and "yttria". Elements 8 (5), 355–360.
Yu, C., Drake, H., Mathurin, F.A., Åström, M.E., 2017. Cerium sequestration and accumulation in fractured crystalline bedrock: the role of Mn–Fe (hydr–) oxides and clay minerals. Geochim. Cosmochim. Acta 199, 370–389.
Zheng, Y.F., 1993. Calculation of oxygen isotope fractionation in anhydrous silicate minerals. Geochim. Cosmochim. Acta 57, 1079–1091.